

This discussion paper is/has been under review for the journal Atmospheric Measurement Techniques (AMT). Please refer to the corresponding final paper in AMT if available.

# Measurement of motion corrected wind velocity using an aerostat lofted sonic anemometer

W. R. Stevens<sup>1,\*</sup>, W. Squier<sup>2</sup>, W. Mitchell<sup>2</sup>, B. K. Gullett<sup>2</sup>, and C. Pressley<sup>2</sup>

<sup>1</sup>Oak Ridge Institute for Science and Education Postdoctoral Fellow to the US Environmental Protection Agency Office of Research and Development, National Risk Management Research Laboratory, Research Triangle Park, NC 27711, USA

<sup>2</sup>US Environmental Protection Agency Office of Research and Development, National Risk Management Research Laboratory, Research Triangle Park, NC 27711, USA

\*now at: Kentucky Christian University, Dept. of Health Sciences, Grayson, KY 41143, USA

Received: 12 December 2012 – Accepted: 16 December 2012 – Published: 21 January 2013

Correspondence to: B. K. Gullett (gullett.brian@epa.gov)

Published by Copernicus Publications on behalf of the European Geosciences Union.

703

## Abstract

An aerostat-lofted, sonic anemometer was used to determine instantaneous 3 dimensional wind velocities at altitudes relevant to fire plume dispersion modeling. An integrated GPS, inertial measurement unit, and attitude heading and reference system corrected the wind data for the rotational and translational motion of the anemometer and rotated wind vectors to a global North, West, Up coordinate system. Data were taken at rates of 10 and 20 Hz to adequately correct for motion of the aerostat. The method was applied during a prescribed forest burn. These data were averaged over 15 min intervals and used as inputs for subsequent dispersion modeling. The anemometer's orientation data are demonstrated to be robust for converting the wind vector from the internal anemometer reference system to the global reference system with an average bias between 5 and 7°. Lofted wind data are compared with sonic anemometer data acquired at 10 m on a mast located near the tether point of the aerostat and with local meteorological data.

## 1 Introduction

Accurate wind velocities are critical inputs for modeling atmospheric dispersion. For buoyant plumes, such as those from combustion sources, the lateral dispersion often occurs at heights well above ground based wind sensors. Additionally, local topography, nearby structures, and the localized convective forces during a fire can make ground based measurements a poor indicator of wind at higher altitudes. Currently, the de facto standard is to use meteorological models (e.g. Weather Research and Forecasting model (WRF)) or ground level meteorological data from nearby weather stations to predict plume wind velocities. However, both of these methods have uncertainties that can lead to unacceptably large errors in downwind plume position in excess of 5 km.

Attempts to determine atmospheric wind velocities beyond the reach of ground based measurements can be categorized as either in situ or remote measurements.

704





### 3 Results and discussion

The data presented here were taken during four flights that measured lofted wind velocities and assessed the motion and orientation correction algorithm. These data were compared with wind data simultaneously acquired at the nearby Val Paraiso meteorological station ([www.ncdc.noaa.gov](http://www.ncdc.noaa.gov)) that would otherwise have been used as inputs for dispersion models. At Eglin AFB, two days of flights lasted between 2 and 4 h and the aerostat height varied between 10 m and 400 m.

Figure 3 shows wind velocity, anemometer, and altitude data acquired on 12 February 2011 at Eglin AFB. The topmost trace is the aerostat altitude measured by the MTi-G, the middle plot is the vertical velocity component, and the bottom trace is a plot of the magnitude of the horizontal wind  $(v_N^2 + v_W^2)^{1/2}$ . Also plotted on the bottom trace are arrows that indicate the direction from which the wind is blowing. Changes in height are a result of maneuvering of the aerostat to maintain its position in the plume from the prescribed forest burn. On both Eglin AFB flights, the altitude of the aerostat was increased to match the plume height increase during the duration of the burn. The low wind speeds ( $< 5 \text{ ms}^{-1}$ ) and changing wind direction in the Eglin AFB data represent unstable to slightly unstable atmospheric conditions. Figure 3b shows unsmoothed 10 Hz data acquired on 12 February 2011 to demonstrate the high temporal resolution of the motion corrected anemometer data.

Figure 4 demonstrates the reliability of the orientation correction of the MTi-G system where  $0^\circ$  is true North. The bottom plot contains 15 min averages motion corrected globally referenced wind vectors and the aerostat tether angle determined from the GPS coordinates of the ground tether point and the aerostat using the Haversine Eqn (Gellert, 1989). The force of the wind upon the aerostat causes the aerostat to act like a wind vane and should therefore provide a reasonable comparison to averaged wind direction data from the sonic anemometer. An average offset between the tether angle and wind velocity data was determined to be  $11^\circ$ , indicating good agreement. Small

709

discrepancies are to be expected due to the ability of the aerostat to rotate about the tether during periods of low wind.

Figure 5 demonstrates the ability of the MTi-G to quickly and reliably determine its orientation in the North-West plane despite potential interferences from onboard sampling equipment. The MTi-G uses magnetometers to determine its orientation in the North-West plane which, due to the weakness of the Earth's magnetic field, could give erroneous readings due to nearby magnetic fields from other sampling equipment on the DASS. The most likely source of magnetic interference is a semi volatile organic hydrocarbon (SVOC) sampling pump co-mounted on the aerostat for pollutant sampling. On Fig. 4, "SVOC flow rate" indicates the operating status of this pump as well as other sampling equipment. When the flow rate departs from its baseline, the sampling equipment is operating and when it remains at the baseline, this equipment is not running (the sampling equipment is triggered by  $\text{CO}_2$  levels). The MTi-G orientation in the North-West plane is directly output from the MTi-G in the form of the  $r_{31}$  and  $r_{32}$ , terms of the  $\mathbf{R}_{GS}$  rotation matrix in Eq. (1). These data were compared with handheld compass readings of the anemometer orientation logged manually every 30 s and the azimuth from the balloon to the tether point (i.e. the tether angle.) Real time aerostat tether angles were calculated from the GPS positions of the anemometer and the tether point using the Haversine Eqn (Gellert, 1989) The tether angle and anemometer orientation should agree as a result of the sail attached to the rear of the aerostat (see Fig. 1) This relationship is qualitative, however, since the aerostat is capable of rotating about the tether in low stability conditions. These rotations are observed as the spikes in the orientation data shown in Fig. 4 at times 17:33, 17:34, and 17:41 UTC. Table 1 shows the compass readings and the 10 point (1 s) average of the MTi-G orientation evaluated at the same time. The differences between these values were averaged to determine the reported average bias of  $5^\circ$ . The orientation values determined at 17:35 UTC were excluded from this calculation as the twisting of the balloon was noted during the measurement.

710

Figure 6 shows a plot of the aerostat wind velocities and altitudes averaged over 15 min with ground wind data acquired at a mast height of 10 m. The green trace represents wind data acquired from a second R. M. Young 81000 3-D sonic anemometer positioned on a 10 m mast near the tether point. These provide a direct comparison to the wind data acquired from the aerostat based anemometer. Data are not shown on 6 February 2011 due to the lack of suitable mast locations near the tether points on this day. The black arrows and points indicate wind direction and speed measured from a nearby airfield. These data were acquired from the NOAA national climatic data center (ValParaiso/Eglin Airfield, [www.ncdc.noaa.gov](http://www.ncdc.noaa.gov)). As expected, wind velocities measured by the aerostat are higher than the wind velocities determined by ground based anemometers. With the exception of the point at 18:00 UTC on 12 February 2011, the Airfield wind speeds are within  $1 \text{ ms}^{-1}$  of the aerostat wind speeds (both are 15-min averages). The aerostat wind directions also generally agree with the ground based anemometer and Airfield met data. However, there was a significant discrepancy between the Airfield and aerostat wind directions on 6 February 2011 of about  $180^\circ$ . It should be noted that the meteorological conditions on 6 February 2011 were somewhat unstable and that this discrepancy could be real. We may therefore speculate that, at least under unstable atmospheric conditions, wind data from nearby meteorological stations may not be a totally reliable proxy for the plume wind velocities.

#### 20 4 Conclusions

A novel method for the measurement of 3-D wind velocities using an aerostat has been reported. Comparison with the ground compass measurements and aerostat position relative to the anchor point showed that the MTi-G's ability to correct for changes in the sonic anemometer orientation relative to the global reference system was about  $\pm 5^\circ$ . Furthermore, wind data acquired from a nearby airfield agreed with local, ground based meteorological stations to within  $1 \text{ ms}^{-1}$ . For all measurements, aerostat wind speeds were higher than ground based speeds. This is likely a result of boundary layer

711

effects associated with the Earth's surface. Significant discrepancies were observed between the aerostat wind directions and both the ground based and nearby airfield wind directions, indicating that wind directions acquired from regional ground based meteorological stations may not sufficiently represent local conditions when precisions greater than 20 degrees are needed.

*Acknowledgements.* The authors would like to acknowledge support for this study from the Environmental Protection Agency (EPA) and Strategic Environmental Defense Program (SERDP). Financial support for W. R. Stevens was provided through a fellowship with the Oak Ridge Institute for Science and Education (ORISE).

#### 10 References

- Aurell, J., Gullett, B. K., Pressley, C., Tabor, D., and Gribble, R.: Aerostat-lofted instrument and sampling method for determination of emissions from open area sources, *Chemosphere*, 85, 806–811, 2011.
- Brooks, I. M.: Spatially distributed measurements of platform motion for the correction of ship-based turbulent fluxes, *J. Atmos. Ocean. Tech.*, 25, 2007–2017, 2008.
- Doyle, J. D., Volkert, H., Dornbrack, A., Hoinka, K. P., and Hogan, T. F.: Aircraft measurements and numerical simulations of mountain waves over the central Alps: a pre-MAP test case, *Q. J. Roy. Meteor. Soc.*, 128, 2175–2184, 2002.
- Frehlich, R., Meillier, Y., Jensen, M. L., and Balsley, B.: Turbulence measurements with the CIREs tethered lifting system during CASES-99: calibration and spectral analysis of temperature and velocity, *J. Atmos. Sci.*, 60, 2487–2495, 2003.
- Gellert, W., Gottwald, S., Hellwich, M., Kästner, H., and Küstner, H.: *The VNR Concise Encyclopedia of Mathematics*, 2nd Edn., Van Nostrand Reinhold, New York, 1989.
- Khelif, D., Burns, S. P., and Friehe, C. A.: Improved wind measurements on research aircraft, *J. Atmos. Ocean. Tech.*, 16, 860–875, 1999.
- Lane, T. P., Reeder, M. J., Morton, B. R., and Clark, T. L.: Observations and numerical modelling of mountain waves over the Southern Alps of New Zealand, *Q. J. Roy. Meteor. Soc.*, 126, 2765–2788, 2000.

712

- Metzger, S., Junkermann, W., Butterbach-Bahl, K., Schmid, H. P., and Foken, T.: Measuring the 3-D wind vector with a weight-shift microlight aircraft, *Atmos. Meas. Tech.*, 4, 1421–1444, doi:10.5194/amt-4-1421-2011, 2011.
- 5 Millane, R. P., Stirling, G. D., Brown, R. G., Zhang, N., Lo, V. L., Enevoldson, E., and Murray, J. E.: Estimating wind velocities in mountain lee waves using sailplane flight data, *J. Atmos. Ocean. Tech.*, 27, 147–158, 2010.
- Shuqing, M., Hongbin, C., Gai, W., Yi, P., and Qiang, L.: A miniature robotic plane meteorological sounding system, *Adv. Atmos. Sci.*, 21, 890–896, 2004.
- 10 Van den Kroonenberg, A., Martin, T., Buschmann, M., Bange, J., and Vorsmann, P.: Measuring the wind vector using the autonomous mini aerial vehicle M(2)AV, *J. Atmos. Ocean. Tech.*, 25, 1969–1982, 2008.

713

**Table 1.** Anemometer orientation and compass values for direct comparison.

| Time<br>(HH:mm:ss)  | Compass<br>(° CCW from N) | MTiG orientation<br>(° CCW from N) | $\Delta$ |
|---------------------|---------------------------|------------------------------------|----------|
| 17:33:30            | 100                       | 100                                | 0        |
| 17:34:00            | 35                        | 27                                 | 8        |
| 17:34:30            | 10                        | 16                                 | 6        |
| 17:35:30            | 10                        | 7                                  | 3        |
| 17:36:00            | 5                         | 10                                 | 5        |
| 17:36:30            | 10                        | 1                                  | 9        |
| 17:37:30            | 15                        | 5                                  | 10       |
| 17:38:00            | 10                        | 12                                 | 2        |
| 17:38:30            | 20                        | 18                                 | 2        |
| 17:39:00            | 23                        | 17                                 | 6        |
| 17:39:30            | 25                        | 25                                 | 0        |
| 17:40:00            | 32                        | 26                                 | 6        |
| 17:40:30            | 15                        | 16                                 | 1        |
| 17:41:00            | 10                        | 7                                  | 3        |
| 17:41:30            | 8                         | 7                                  | 1        |
| 17:42:00            | 2                         | 3                                  | 1        |
| 17:42:30            | 8                         | 13                                 | 5        |
| 17:43:00            | 8                         | 6                                  | 2        |
| 17:43:30            | 2                         | 27                                 | 25       |
| Average Difference: |                           |                                    | 5°       |

714



**Fig. 1.** Photograph of Aerostat based sampling system equipped with the 3-D anemometer mounted below the samplers.

715

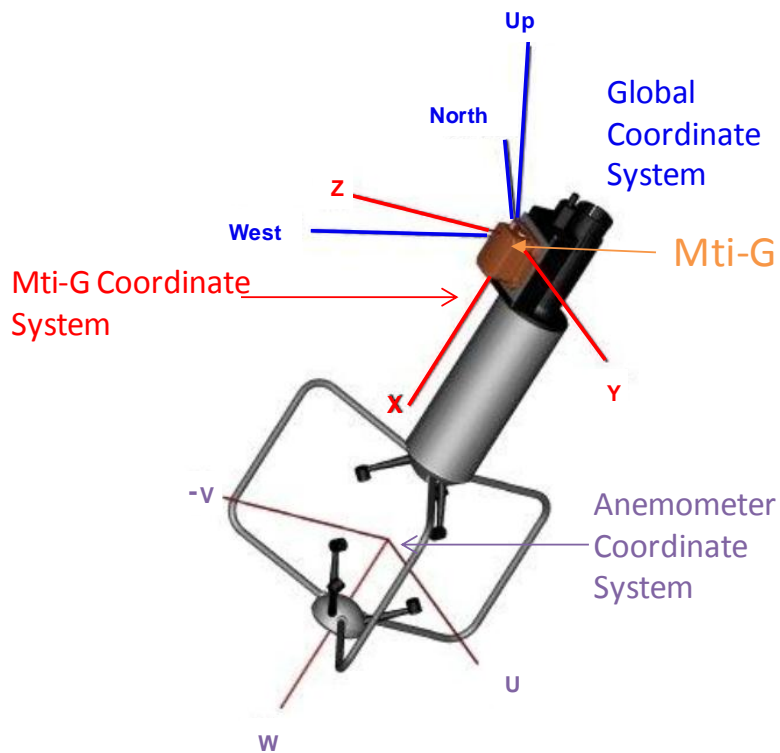


**Fig. 2.** Sonic Anemometer/MTi-G schematic. Note that  $U$  axis of the anemometer is aligned with the  $Y$  axis of the MTi-G,  $-V$  is aligned with  $Z$ , and  $W$  is aligned with  $X$ . The MTi-G determines the  $\mathbf{R}_{GS}$  rotation matrix to convert from the MTi-G/sonic anemometer reference frame to the North, West, Up global coordinate system.

716

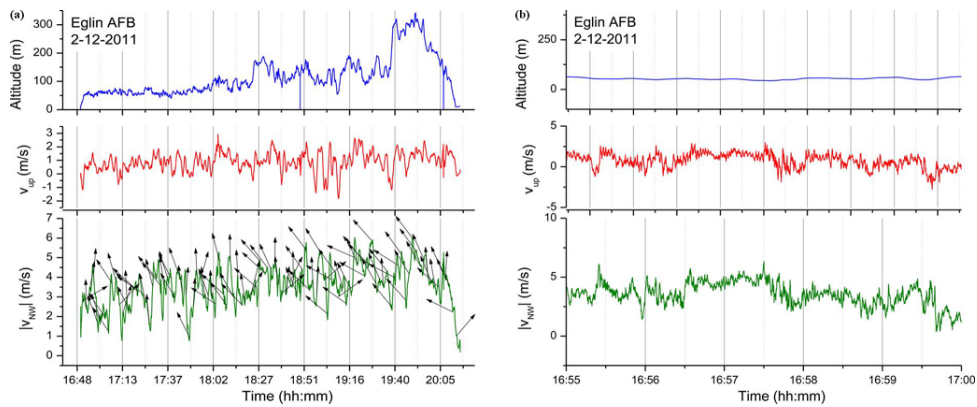


**Fig. 3.** Wind data from 12 February 2011. The topmost trace (blue) represents the aerostat altitude as measured by the MTi-G. The middle trace (red) is the motion corrected and rotated vertical wind velocity component. The bottom trace (green) indicates horizontal wind speed defined as  $(V_N^2 + V_W^2)^{1/2}$ . The black arrows in (a) indicate the wind direction where up is north and left is west. The data in (a) are smoothed using a rolling average with a window of 60 s. The data in figure (b) are unsmoothed 10 Hz data.

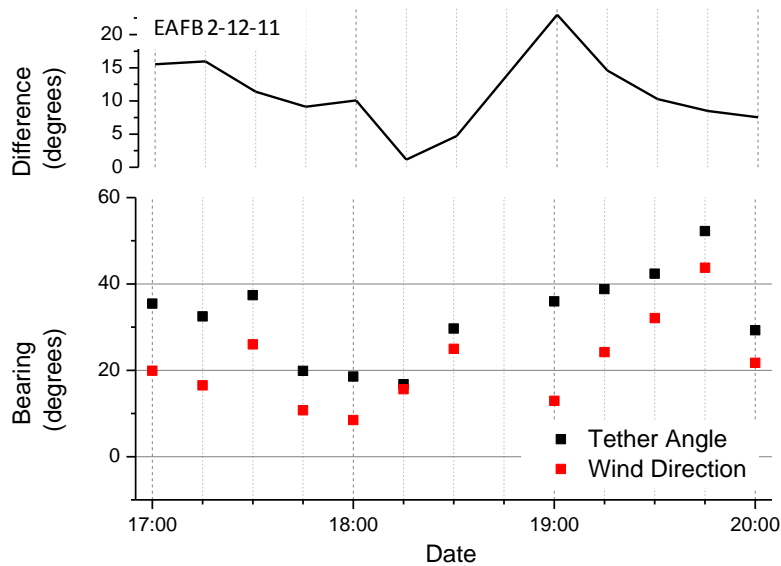


**Fig. 4.** Wind Direction vs. Tether Angle. Points (bottom graph) indicate 15 min averages of wind direction and tether angle where 0° corresponds to true north. The black line (top) corresponds to the difference between the average tether angle and wind direction.



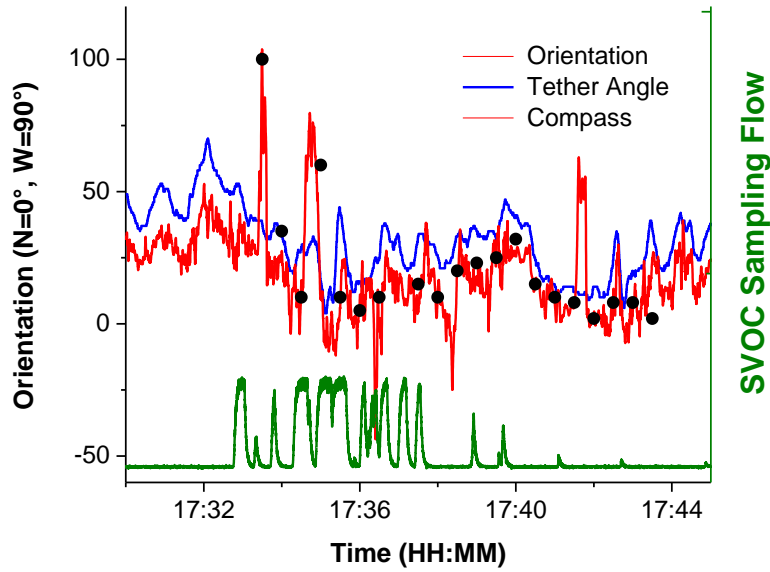


**Fig. 5.** Anemometer orientation (red), Aerostat tether angle (blue), plotted with compass reference points (●) where 0 corresponds to the anemometer facing north. The SVOC sampling flow rate (green) indicates the status of the onboard sampling equipment and the potential existence of transient magnetic fields which is shown to not confound the orientation measurements.

719

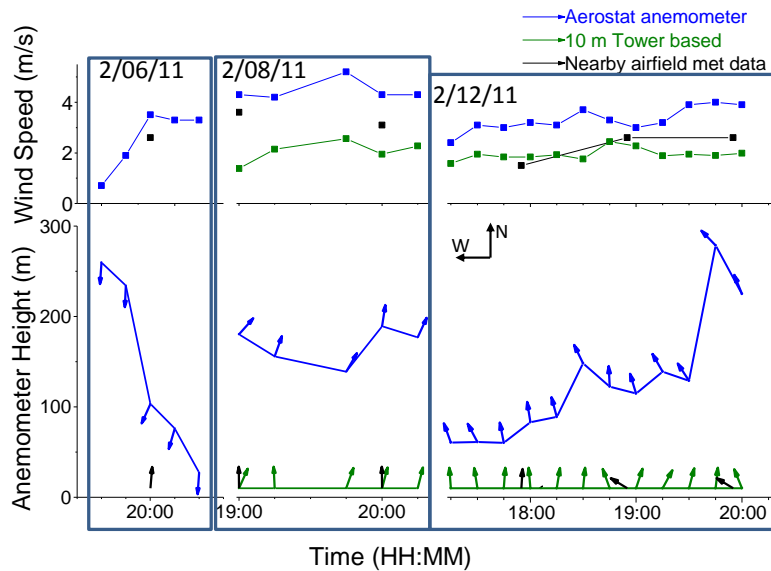


**Fig. 6.** Wind directions plotted at the height and time of day acquired (bottom) and magnitudes (top) observed from the Aerostat based anemometer (blue), ground 3-D sonic anemometer mounted to a 10 m tower (green), and 2-D anemometer located at a nearby airfield reported to the NOAA weather archive (black). Arrows indicate the direction from which the wind is blowing where north is up and west points to the left.

720